Organic Rankine Cycle with Direct Liquid Injection into a Twin-Screw Expander

Sebastian Eyerer [a], Florian Rieger [a,b], Fabian Dawo [a], Andreas Schuster [b], Richard Aumann [b], Fabian Kricke [b], Roy Langer [b], Christoph Wieland [a] and Hartmut Spliethoff [a,c]

[a] Technical University of Munich, Institute for Energy Systems, Garching, Germany,
sebastian.eyerer@tum.de, CA
[b] Orcan Energy AG, Munich, Germany
[c] Bavarian Center for Applied Energy Research, Garching, Germany

Abstract:

The Organic Rankine Cycle (ORC) is a thermal engine, which is applied to convert low temperature heat to electrical power using organic working fluids. It is an established technique for waste heat recovery, as well as for the utilization of biomass, geothermal energy and solar energy. This study presents a novel operational strategy of an ORC, which allows for reliable control of process parameter while simultaneously ensuring a high cycle efficiency. This strategy is analyzed experimentally and compared with a system simulation. With this method, preheated liquid working fluid is injected to partially expanded vapor inside a volumetric screw expander. The injected mass flow bypasses the evaporator and can be controlled by a valve. Thus, the direct liquid injection into the expander reduces the exhaust temperature, reducing the risk of thermal damages in case of a hermetic or semi-hermetic expander. The experimental and simulation results show, that the exhaust vapor temperature can be reduced by approx. 40 K for the investigated operation conditions. This enables the expander to run at higher live steam conditions by simultaneously ensuring sufficient cooling of the generator and thus allows for higher power production. Alternatively, lower exhaust temperatures lead to the advantage of less required desuperheating in the condenser and thus to higher overall heat transfer coefficients in the condenser, allowing for smaller heat transfer areas.

Keywords:

Control strategy, Direct liquid injection, Screw expander, Experimental study, Modelling, Performance optimization.

1. Introduction

Within the last 20 years, the primary energy consumption increased by more than 50 %. This led to an increase in CO_2 emissions of approximately 50 % within this period [1]. Based on this development, the goal of the Paris Agreement of the UN framework convention on climate change is to limit the increase in global average temperature to 2 °C above pre-industrial levels [2]. Therefore, considerable efforts to increase the share of renewable energy sources for power and heat production (1), to improve the use of waste or low-temperature heat sources (2), and to increase the energy efficiency on the demand side (3), are made to reduce overall global greenhouse gas emissions.

In this context, the Organic Rankine Cycle (ORC) is a promising technology focusing on the above-mentioned first and second approach of reducing CO_2 emissions. The ORC enables low-temperature heat sources to be used for power generation and can thus be applied to industrial waste heat and renewable sources such as solar heat, geothermal brine or biomass combustion.

In small to medium scale ORC systems, typically volumetric expanders, such as scroll or screw expanders, are used [3-5]. There are three different construction types how to enclose the expander and the generator [6]. For the open construction type, the expander and the generator are two separate components without any common enclosure. The expander shaft then goes through the casing using an appropriate seal. In the opposite, the hermetic construction type features one common housing for expander and generator, building a closed cabinet. The third type is the semi-hermetic construction, where expander and generator are inside one common housing, but the housing can be opened e.g.

for maintenance purposes. The semi-hermetic and the hermetic construction type features many advantages over the open type such as a high compactness, lower refrigerant leakage and lower maintenance effort. However, cooling of the generator is typically ensured, by using the exhausted vapor from the expander as cooling medium. Typical maximal temperatures of the generator windings are in the rage of 110 to 125 °C. In order not to exceed these manufacturers' requirements, the exhaust vapor temperature should be in the range of 75 °C to 90 °C. This in turn, limits the live vapor parameter and thus the power output and the efficiency of the system.

To overcome this limitation and to enable the system to run at higher live vapor parameter, a novel operational strategy, the direct liquid injection (DLI) into the expander, is presented in the publication. This procedure has already been patented [7] by Orcan Energy AG. The purpose of this work is to evaluate the DLI using both, simulative and experimental investigations.

Therefore, the basic functionality of the DLI and its effect on the expansion process are explained at first. After that, the experimental methodology and the simulation procedure are described. Then, the experimental and simulative results are presented and discussed, in order to finally evaluate the performance of the direct liquid injection.

2. System description and basic functionality

In this section, the operational strategy of the direct liquid injection (DLI) is presented and relevant effects are discussed. Therefore, some fundamentals of volumetric expanders are shortly introduced, in order to better explain the effect of the DLI on the expansion process.

The basic layout of the direct liquid injection is depicted in Fig. 1 (a) and the corresponding temperature-entropy diagram is shown in Fig. 1 (b). The layout of the DLI is quite similar to a basic ORC layout comprising a pump, heat exchanger for preheating, evaporation and superheating, an expansion machine and a condenser. The major difference is the connection between preheater and expander, where preheated liquid working fluid is directed into the expander at an intermediate pressure stage. The mass-flow towards the expander is thereby controlled by the valve between the state ③ and ⑥ in Fig. 1. In the expander, the liquid fluid is mixed with the superheated vapor at state ⑤, such that the injected flow evaporates by cooling the superheated vapor. The exhaust vapor at state ⑧ has thus a lower temperature compared to the case without DLI.

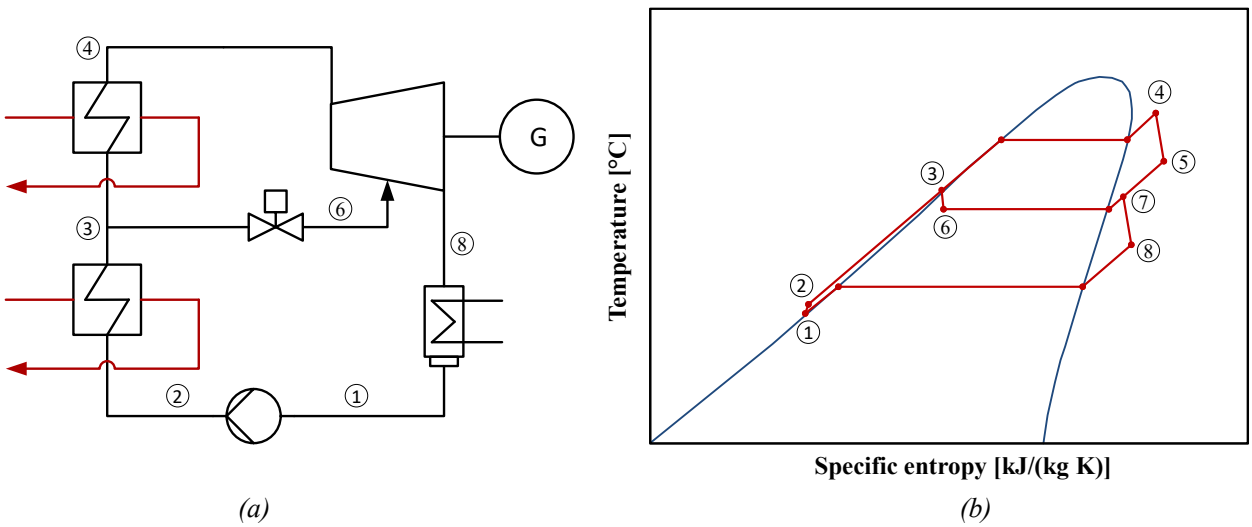

(a) *(b)*

Fig. 1. ORC with direct liquid injection: a) layout of the system, b) temperature-entropy diagram.

In order to understand the expansion process with the DLI better, Fig. 2 shows the corresponding pressure-volume diagram. In general, the expansion process is volumetric expanders, such as screw expanders, is dominated by the build-in volume ratio φ_i of the expander. This ratio is defined as the

ratio between the volume of the working chamber at the end and the beginning of the expansion, corresponding with the respective volumes at state ⑦ and ② in Fig. 2. If the system specific volume ratio, which is defined by the live vapor and the condensation states, is larger than the build-in volume ratio of the expander, under expansion occurs. There, the pressure at the end of the expansion process is larger than the pressure in the discharge line. This case is depicted in Fig. 2 between the states ⑥ and ⑦. In the case where the specific volume ratio is lower than the build-in volume ratio, over-expansion occurs, where the fluid at the end of the expansion process is recompressed to the higher pressure in the discharge line. These two effects considerably reduce the efficiency of the expansion process compared to a perfect expansion, where the pressure at the end of the expansion process equals the pressure in the discharge line.

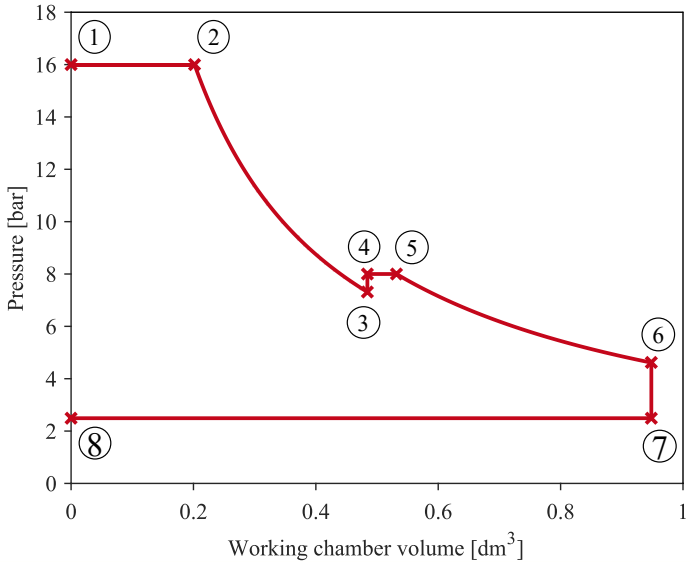

Fig. 2. Pressure-volume diagram of the expansion process with direct liquid injection.

Looking now at the expansion process of the DLI, the first step between states ① and ② in Fig. 2 is the admission of the fluid into the working chamber. The working chamber volume than increases due to the rotation, progressively expanding the fluid from state ② to ③. At the corresponding working chamber volume of state ③, the injected fluid enters the expander. Thereby, the admission port of the DLI opens progressively with advancing volume along the screw. Due to the higher pressure in the injection line, the pressure inside the expander increases. This procedure can be modelled with a isochoric increase in pressure from state ③ to ④ and a isobaric increase in volume from state ④ to state ⑤ [8]. The increase in pressure is an indicator for the amount of injected mass. Since the volume does not change, a higher pressure leads to a higher density and thus a larger mass in the working chamber. Since the position of the DLI is not infinitesimal small, but is a borehole with approx. 5-8 mm diameter, the volume of the working chamber slightly increases during injection process, due to further rotation of the screws. This step from state ④ to state ⑤, where also the mixing of the injected flow takes place, is considered isobaric. Afterwards, the fluid in the working chamber is expanded from state ⑤ to ⑥, similar to the process from state ② to ③. The major difference is now, that the mass of the second expansion step is larger than the mass in the first expansion step. From state ⑥ to ⑦ the under-expansion, as described above, is shown. The last step, from state ⑦ to ⑧ is the discharge of the fluid into the discharge line.

3. Experimental facility and methodology

In order to demonstrate the DLI, the above-described ORC setup has been implemented using a twin-screw expander. The used experimental setup with all options for controlling the process parameters is described in this section. Furthermore, the applied measurement devices as well as their accuracy are specified. Finally, the experimental procedure is presented.

3.1. ORC system and control options

The ORC system, used for the experimental investigation, has the layout shown in Fig. 1 (a). A photograph of the experimental setup is shown in Fig. 3. Besides the actual ORC loop, a heating loop, were distilled water circulates, is applied as heat source for the ORC. Both loops are connected by the evaporator and the preheater. The working fluid used for the experiments is R245fa. In order to set the appropriate operational conditions, five main parameters can be controlled: the heat source temperature and thus the live vapor temperature, the rotational speed of the expander, the working fluid mass-flow rate, the condensation pressure and the injected mass-flow rate.

Fig. 3. ORC system used for the experimental investigation.

The heat source of the ORC consists of an electrical resistance heater with a maximum power of 330 kW, which is controlled by a pulse width modulation such that a constant temperature at the evaporator inlet can be ensured. The applied expander is a twin-screw compressor, which is modified to work as expander. The injection port is placed at a volume ratio, which corresponds to 51 % of the build-in volume ratio of the expander. In order to ensure proper lubrication of all bearings and sealing between the screws itself and between the screws and the housing, a certain amount of refrigerant oil is added to the working fluid to circulate in the ORC loop such that the live vapor contains an oil spray. The speed control is ensured by using an inverter and the produced electrical power is discharged via an electrical load bank. The ambient air is used as a heat sink for the test rig. Therefore, the air mass flow through the plate-fin air-cooled condenser is adjusted via a speed-controlled fan so that a desired condensation temperature and the corresponding condensation pressure can be achieved.

Table 1. Measuring range and accuracy of applied sensors.

Measured parameter	Physical principle of measurement	Measuring range	Accuracy of measurement
Pressure	Strain gauge	0 to 25 bar	0.5% of MV + 1.3% of EV
Temperature	PT100	-50 to 200 °C	±0.3 °C + 0.05% of MV
Total working fluid mass-flow rate	Coriolis sensor	0.1 to 2 kg/s	±0.15% of MV
Injected volume-flow rate	Positive displacement sensor	15 to 550 l/h	±1% of EV
Electrical gross power output	Power meter	0 to 35 kW	±2% of EV

The ORC system is fully instrumented, having temperature and pressure sensors before and behind each component, measuring the total and the injected mass-flow rate as well as having sensors for electrical power measurement. All the instrumentation and measuring ranges as well as the accuracy of each sensor is summarized in Table 1. Using the measured values, further relevant properties such as enthalpy, entropy and density are calculated with Refprop 9.1 [9]. The measured values, together with the calculated fluid properties, are used to obtain characteristic process parameters.

3.2. Methodology of experiments

For an objective and comprehensive evaluation of the DLI, in total 108 stationary operation points where investigated. Therefore, one of the controllable parameters live vapor temperature, condensation pressure, rotational speed of the expander or injected mass-flow rate is varied while all others are kept constant. The investigated live vapor temperatures are 120 °C, 113 °C and 106 °C. The rotational speed is changed from 3300 rpm, over 3000 rpm to 2700 rpm and the condensation pressure is varied between 2.5 bar, 3.0 bar and 3.5 bar. The inlet temperature of the preheater was controlled to be 85 °C in all cases. This results in 27 operation points of the ORC system without direct liquid injection and thus serve a benchmark for the investigation. For the DLI, three different injection mass-flow rates (0.1 kg/s, 0.2 kg/s and 0.3 kg/s) are tested for each of the above described operation condition. This ensures that the DLI is investigated in a huge operation range of the system, including full and part-load operation. For all operating points, stationary conditions are maintained for at least 10 min. For data evaluation, every 10 s a measurement value is acquired for each sensor. For one stationary operation point, all values of a sensor within the last five minutes are averaged, to obtain a meaningful value for this operation point.

4. Simulation of the DLI and validation of the model

This section provides the description of the simulation model, which has been implemented in the commercial software package Engineering Equation Solver (EES). This software package is able to solve a huge number of equations using a numerical solution algorithm. Furthermore, the validation of the model with the above-mentioned experimental data is presented.

In order to create the model of the investigated ORC with direct liquid injection (DLI) into the expander several assumptions were made. The whole process is assumed adiabatic and pressure losses are only taken into account for the heat exchangers. The working fluid R245fa is treated as a pure fluid, which means the circulating oil in the cycle is neglected. Table 2 summarizes the remaining boundary conditions and defined parameters of the model.

Table 2. Boundary conditions and defined parameters of the model.

Evaporator		Condenser	
Water inlet temperature	140 °C	Air inlet temperature	15 °C
Water inlet pressure	5 bar	Air inlet pressure	1.103 bar
Superheating	7 K	Subcooling	15 K
Preheater		Expander	
Water inlet temperature	85 °C	Isentropic efficiency	0.80
Water inlet pressure	4 bar	Generator efficiency	0.9

The effectiveness-NTU method [10] is used to calculate the heat exchangers. The effectiveness of the heat exchanger ε is defined as the quotient of actually transmitted heat flow $\dot{Q}$ and maximum possible transmitted heat flow $\dot{Q}_{max}$:

$$\varepsilon = \frac{\dot{Q}}{\dot{Q}_{max}}. \quad (1)$$

In order to calculate the maximum possible transmitted heat, the heat capacity flow of the hot and the cold stream $\dot{C}_{h/c}$ and the maximum temperature difference in the heat exchanger are calculated as follows:

$$\dot{C}_{h/c} = c_{p,h/c} \cdot \dot{m}_{h/c} \begin{cases} if\ \dot{C}_h > \dot{C}_c \rightarrow \dot{C}_{min} = \dot{C}_c, \dot{C}_{max} = \dot{C}_h \\ if\ \dot{C}_c > \dot{C}_h \rightarrow \dot{C}_{min} = \dot{C}_h, \dot{C}_{max} = \dot{C}_c \end{cases}, \quad (2)$$

$$\Delta T_{max} = T_{h,in} - T_{c,in}, \quad (3)$$

$$\dot{Q}_{max} = \dot{C}_{min} \cdot \Delta T_{max}. \quad (4)$$

The efficiency of the heat exchanger is a function of the ratio of the heat capacity flows and the number of transfer units *NTU* and depends on the heat exchanger type (counter-current, co-current, crosscurrent flow, cross flow). In this case, the counter-current operation is implemented:

$$\varepsilon = \frac{1-exp(-NTU\cdot(1-\dot{C}_r))}{1-\dot{C}_r\cdot exp(-NTU\cdot(1-\dot{C}_r))}, \quad (5)$$

$$NTU = \frac{A\cdot U}{\dot{C}_{min}}, \quad \dot{C}_r = \frac{\dot{C}_{min}}{\dot{C}_{max}}. \quad (6)$$

If ε and $\dot{Q}_{max}$ are determined, the actual transferred heat flow can be determined from (1). This procedure is used for all modelled heat exchangers. While it can be used straight forward for the preheater, the evaporator and the condenser have to be split in three parts, because different heat transport phenomena occur in these components. The evaporator is divided into a first part where preheating until saturation takes place, a second part where the actual evaporation occurs and a third part where the fluid is superheated. Analogously, the condenser is divided in a desuperheating, condensing and subcooling part. In contrast to the preheater and the evaporator, the condenser is operated as a cross flow heat exchanger. In this case, the effectiveness is calculated as:

$$\varepsilon = 1 - exp[\frac{1}{\dot{C}_r} \cdot NTU^{0.22} \cdot (exp(-\dot{C}_r \cdot NTU^{0.78}) - 1)]. \quad (7)$$

The fraction of heat transfer area of the whole condenser area needed for the different parts of the condenser is assumed equal to the fraction of air mass-flow of the whole air mass-flow, which is needed to transfer the appropriate amount of heat. The overall heat transfer coefficient *U* is anticipated to be the same for all three parts of the condenser, because it is determined by the lowest heat transfer coefficient, which is the convective heat transfer to the air. This heat transfer coefficient is calculated by an empirical equation depending on the air mass-flow and the air temperature. In order to determine the auxiliary power demand of the system, the fan power of the cooling system P_{fan} is determined with an empirical polynomial as a function of the rotational speed of the fan n_{fan}:

$$P_{fan} = a_{fan} \cdot n_{fan}^3 + b_{fan} \cdot n_{fan}^2 + c_{fan} \cdot n_{fan}. \quad (8)$$

The power demand of the pump P_p is calculated as:

$$P_p = \frac{\Delta p_p}{\eta_p} \cdot \frac{\dot{m}_{tot}}{(\rho_{in,p}+\rho_{out,p})/2}. \quad (9)$$

The power demand of the water pumps and the remaining electrical parts such as the process control system are assumed to be constant and amount to 1 kW. Pressure losses in the different heat exchangers are considered as a function of the ratio between actual and design (index *D*) volume flow:

$$\Delta p = \Delta p_D \cdot \left(\frac{\dot{V}}{\dot{V}_D}\right)^2. \quad (10)$$

Due to the importance of the expander for the overall process, its modelling is given particular value. The applied expander model is adapted from [11] and allows for the calculation of the internal leakage

in the expander. Fig. 4 illustrates the general procedure for the expander model. First, the live vapor mass flow is separated in a leakage mass flow $\dot{m}_{leak}$ and an internal mass flow $\dot{m}_{int}$, which is utilized for the actual power generation. The ratio of the leakage and the internal mass flow is determined by an empirical equation using a second- order polynomial of the rotational speed and the pressure difference over the expander.

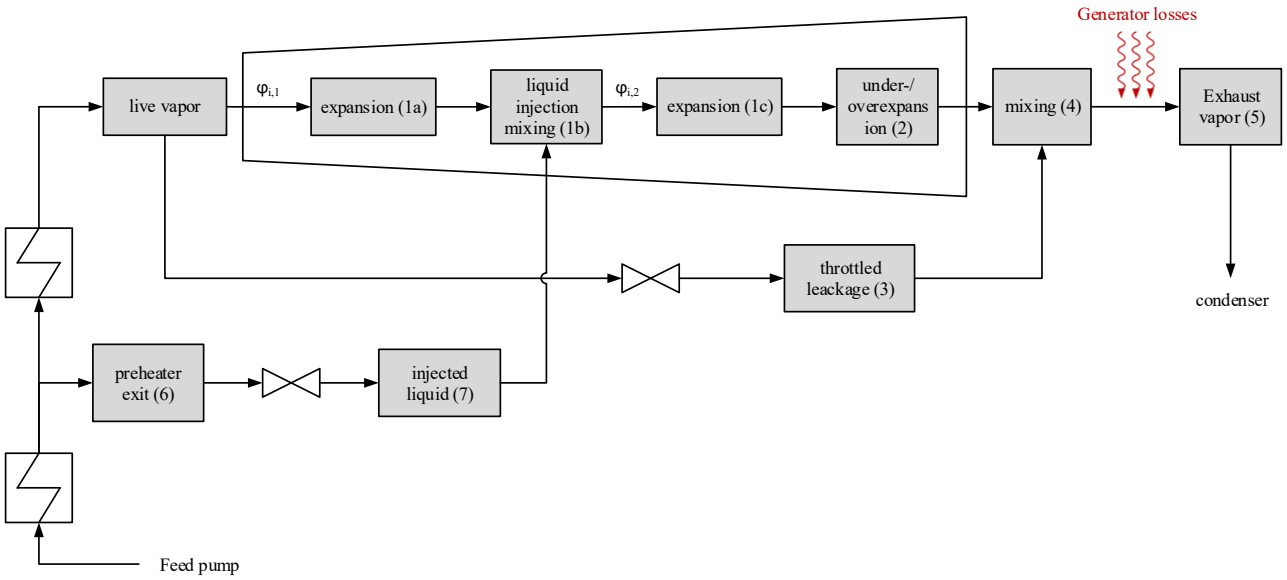

Fig. 4. General scheme for expander model.

The rotational speed of the expander n_{exp} is calculated with the internal volume flow and the swept volume of the expander:

$$n_{exp} = \frac{\dot{V}_{int}}{V_{swept}}. \qquad (11)$$

The implementation of the liquid injection model is done by dividing the expander model into two consecutive expansion steps (cf. (1a) and (1c) in Fig. 4), which are modeled analogously. These steps correspond with the state changes ② - ③ and ⑤ - ⑥ in Fig. 2. The build-in volume ratio φ_i is split up into two parts, while $\varphi_{i,1}$ is valid for the expansion before the liquid injection and $\varphi_{i,2}$ for the expansion after the liquid injection. They are related by the following equation:

$$\varphi_i = \varphi_{i,1} \cdot \varphi_{i,2}. \qquad (12)$$

The internal flow through the expander passes four steps. First, the state after the first expansion (1a) is defined by the live vapor state (index *lv*), the volume ratio of the first expansion $\varphi_{i,1}$ and the isentropic efficiency of the expansion process $\eta_{exp,s}$. Therefore, the enthalpy h_{1a} and the specific volume v_{1a} at that state are calculated as follows:

$$\eta_{ex,s} = \frac{h_{lv} - h_{1a}}{h_{lv} - h_{1a,s}}, \qquad (13)$$

$$v_{1a} = \varphi_{i,1} \cdot v_{lv}. \qquad (14)$$

Based on this, the mechanical power of the first expansion step is determined as follows:

$$P_{mech,Ex,1} = \dot{m}_{int,1} \cdot (h_{lv} - h_{1a}). \qquad (15)$$

In the second step, the mixing of the internal flow after the first expansion (1a) with the injected liquid form the preheater exit (7) occurs in the step (1b) (cf. Fig. 4). This step is followed by the second expansion (1c), which is modeled analogous to the first expansion with the corresponding internal volume ratio $\varphi_{i,2}$, the isentropic efficiency of the expansion process $\eta_{exp,s}$ and the higher mass-flow rate $\dot{m}_{int,2} = \dot{m}_{int,1} + \dot{m}_{inj}$. Finally, the state of the internal flow after the under- or over-

expansion (2) is calculated, which is defined by the pressure after the second expansion p_{1c} and the pressure of the discharge line p_{dis}:

$$P_{mech,over-ex} = \dot{m}_{int,2} \cdot (p_{1c} - p_{dis}) \cdot v_{1c}. \qquad (16)$$

The leakage stream is throttled isenthalpic to the pressure of the exhaust vapor (3) and then mixed with the internal stream (4) (cf. Fig. 4). As the exhaust vapor is used to cool the generator windings, it heats up in turn by the transmitted heat flow $\dot{Q}_{gen}$. The heat flow is calculated using the generator efficiency η_{gen} and the mechanic power of the expander $P_{mech} = P_{mech,Ex,1} + P_{mech,Ex,2} + P_{mech,over-ex}$:

$$\dot{Q}_{gen} = (1 - \eta_{gen}) \cdot P_{mech}. \qquad (17)$$

The exhaust state of the expander model (cf. state (5) in Fig. 4) is determined using a simple energy balance, which includes the generator heat flow.

The above-mentioned parameters and boundary conditions of the simulation model are summarized in Table 2.

The validation of the simulation model is done with experimental data. Several operation points were investigated (cf. section 3.2), whereby water temperature of the evaporator inlet, rotational speed of the expander and condensation pressure were varied. So, for the first validation procedure, the experiments without injection are used. In order to achieve the best possible agreement between model and experimental data the mean overall heat transfer coefficient of the evaporator U_{evap}, the isentropic efficiency of the expander $\eta_{exp,s}$ and the design volume-flow rate of the air in the condenser $\dot{V}_{air,design}$ are fitted. The validation of the ORC model with direct liquid injection is exemplarily shown in Fig. 5 for the exhaust vapor temperature and the gross power output. These two values are chosen because they are the most interesting for the DLI model. The comparison shows that the simulated gross power output is in good agreement with the experimental data. However, the model systematically underestimates the exhaust vapor temperatures slightly. In Fig 5. a deviation tolerance of ± 5% is indicated. In the case of the temperature, the deviation is referred to the Kelvin scale.

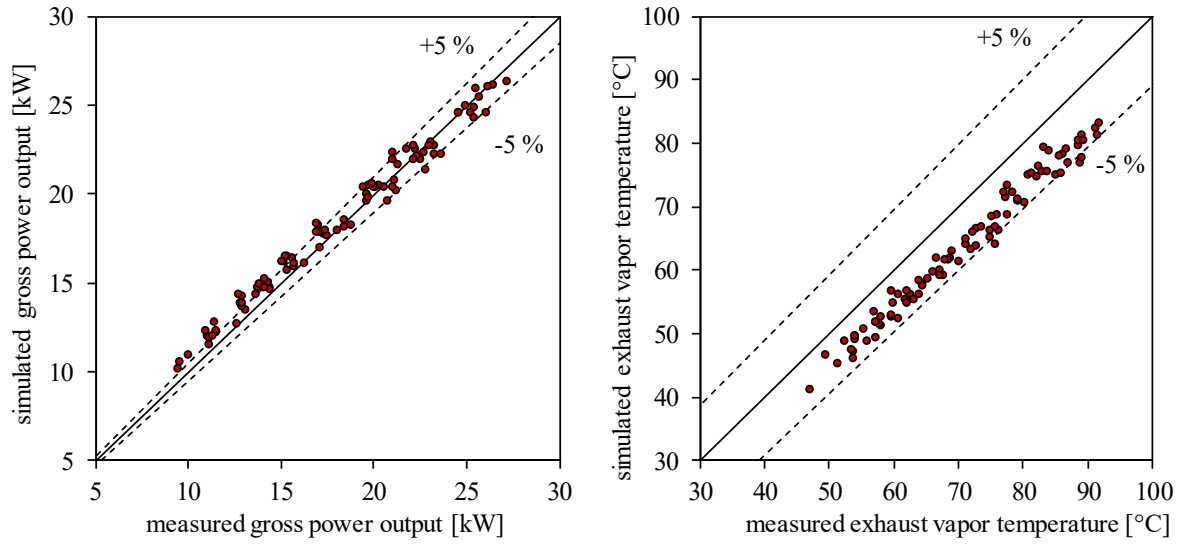

Fig. 5. Comparison between measured and simulated values: a) gross power output, b) exhaust vapor temperature

5. Results and discussion

With the validated simulation model and the experimental procedure described above, the liquid direct injection will be investigated and the effects on the system power output and the exhaust vapor

temperature will be analyzed. At first, the influence of the injected mass-flow rate will be analyzed by using the experimental data and the simulation model. Then, the influence of the DLI position will be investigated in a parameter study using the simulation model. Finally, the capability to increase the live vapor state while simultaneously ensuring adequate exhaust vapor temperatures is shown using the simulation model.

5.1. Influence of the injected mass-flow rate

In this section, the influence of the injected mass-flow rate is analyzed. Therefore, the experimental results for part-load operation with a live vapor temperature of 113 °C, a rotational speed of the expander of 3000 rpm and a condensation pressure of 2.5 bar are depicted in Fig. 6. There, the influence of the injected mass-flow rate on gross power and exhaust vapor temperature is illustrated by showing both, the experimental data and the simulation results. For the experimental data, the measurement errors are calculated using the data in Table 1 and the Gaussian law of error propagation. In the applied expander, the injection port is placed at a volume ratio, which corresponds to 51 % of the build-in volume ratio. This value is also used for the simulations. It can be seen, that the measured gross power output is almost unaffected by the higher injected mass-flow rate. The same is observed with the simulation model. Due to the constant live vapor temperature, controlled in the experiments, also the live vapor mass-flow rate is kept constant. That means that the mass-flow rate after the DLI increases with increasing injected mass-flow rate. This increased flow rate is supposed to cause higher gross power output; however, this effect is compensated by the reduced expander efficiency when using the DLI. Furthermore, it can be seen, that the simulated values for the gross power output are all within the accuracy of the measurements. In case of the exhaust vapor temperature, a significant reduction from 82 °C to 45 °C has been measured with increasing injection flow-rate. This trend can also be observed for the simulation model; however, the simulated values are approx. 5 K lower than the measured values. This investigation proves that a substantial reduction of the exhaust vapor temperature can be achieved by liquid injection, with almost no change in gross power output.

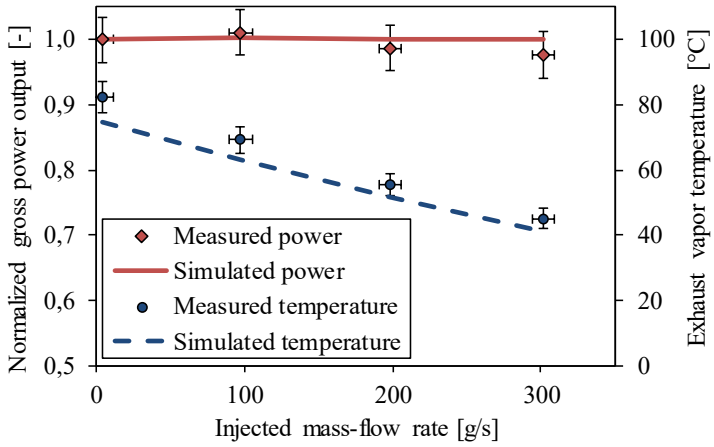

Fig. 6. Influence of injected mass-flow rate on gross power output and exhaust vapor temperature.

5.2. Influence of the position of the direct liquid injection

Besides the amount of injected mass-flow, the position where the injection pipe is connected plays an important role in terms of power output. Since the used expander has a fixed DLI connection, the influence of the position of this connection can only by studied using the simulation model. In order to provide a comprehensive picture, the net power output will be analyzed in this section. Therefore, another part-load operation condition with a live vapor temperature of 120 °C, a rotational speed of the expander of 3000 rpm and a condensation pressure of 3 bar is investigated. In Fig. 7 the influence of the position as well as the injected mass-flow rate on the net power output is depicted. It can be observed, that the net power drops for all positions of the DLI connection with increasing injected mass-flow rate. This is in contrast to the gross power output, which is almost unaffected by the

injection rate (cf. Fig. 6). Since the mass-flow rate through the evaporator and the live vapor state is constant during this variation, the increasing injection rate is caused by a higher mass-flow rate delivered by the supply pump and thus leads to a higher power demand of the pump. Additionally, the power demand of the condenser fans increases. Although the net power drops for all positions of the DLI connection, an interesting effect can be detected in Fig. 6. Looking at one injection rate, a local maximum can be observed, depending on the position of the injection. Regardless of the DLI position, the mixture of preheated and partially expanded fluid causes a decrease in the enthalpy of the internal flow and thus has a negative impact on the enthalpy difference. In contrast, the mass flow of the second expansion increases with higher injection quantities. Thus, the reason for the optimal DLI position can be explained by the opposite effects of the increasing mass-flow rate of the second expansion and the decreasing enthalpy difference due to the mixing with the colder injected mass flow. Thereby, it can also be explained, why a higher injected mass-flow rate causes a more pronounce local maximum. To conclude, the location of the injection port should be chosen carefully to get the maximum possible net power output.

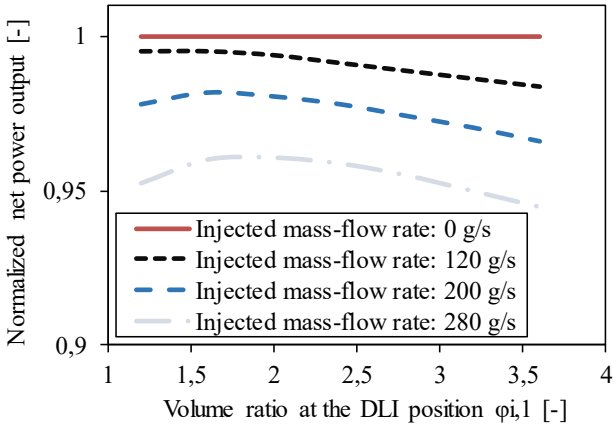

Fig. 7. Influence of the position of the liquid injection on the net power output.

5.3. Capability to increase the live vapor state

The sections 5.1 and 5.2 show that the DLI is able to reduce the exhaust vapor temperature significantly but simultaneously leads to a reduction in net power output. As mentioned above, the live vapor parameters are limited for hermetic and semi-hermetic expanders by the need to cool the generator sufficiently with the exhaust vapor. To overcome this limitation the DLI can be used, enabling the ORC system to run at higher live vapor conditions. In this section, the validated simulation model is used to analyze the influence of the increased live vapor pressure on the net power output. For each live vapor pressure, the necessary injection flow rate is calculated to ensure an exhaust vapor temperature of 80 °C. Since the simulation model underestimates the exhaust vapor temperature (cf. section 4 and Fig. 5b), the real temperatures are expected to be approx. 5 K - 10 K higher. These temperatures are sufficient to the keep the temperature of the generator windings below 120 °C.

For the analysis of this measure, part-load operation condition with a live vapor temperature of 120 °C, a rotational speed of the expander of 3300 rpm and a condensation pressure of 3.5 bar is investigated and serves as a benchmark to evaluate the increase live vapor conditions. The position of the DLI port is set to 51 % of the build-in volume ratio, as it is applied in the experimental investigations. For constant live vapor states, the exhaust vapor temperatures of the expander increase with increasing condensation pressure, due to less amount of post expansion (cf. Fig. 2). Therefore, this reference conditions cause the highest exhaust vapor temperatures of all investigated operation points (cf. Fig. 5b). Figure 8 shows the simulation results keeping the rotational speed and the condensation pressure at the reference conditions. The live vapor parameters are increased stepwise,

while the necessary injection flow rate to keep the exhaust vapor temperatures constant is determined. It can be seen that the net power output can be significantly increased by the increased live vapor conditions for this operation point. The observed increase in net power output is in the range 40 % compared to the reference state without injection. This is caused by a potential increase in live vapor pressure of 6 bar. Furthermore, it can be seen, that only a small injected mass-flow rate of less than 100 g/s is necessary to ensure proper cooling of the generator windings. In this analysis, a maximum live vapor pressure of 22 bar, corresponding with a maximum live vapor temperature of 134 °C (7 K superheating) has been investigated. Higher live vapor states are generally possible, but then potential limitations on the suction side of the expander have to be considered.

When interpreting the above findings, it has to be considered, that the huge increase in power production is only possible if the live vapor parameter are limited by the exhausted vapor temperatures and are thus lower than the thermodynamically optimized parameter for the considered heat source. Furthermore, the higher power output also requires higher thermal power from the heat source, however, possible limitation caused by the heat source are not considered in the simulation.

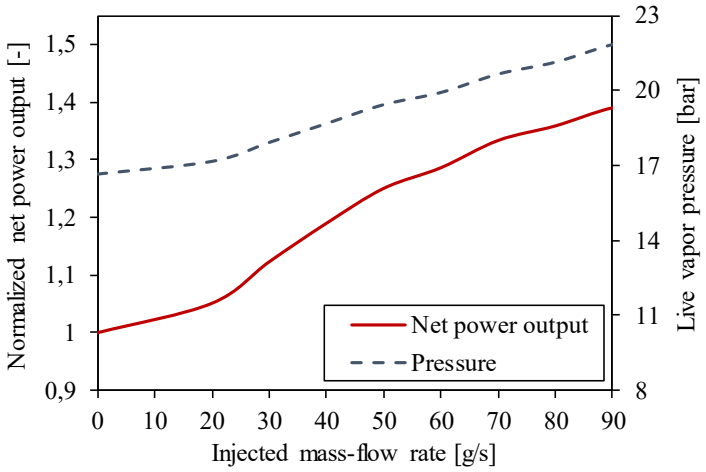

Fig. 8. Net power output and live vapor pressure in dependence of the injected mass-flow rate for constant exhaust vapor *temperatures of 80 °C.*

6. Conclusions

In this paper, the direct injection of liquid working fluid into a screw expander of an Organic Rankine Cycle system has been presented. With this method, preheated liquid working fluid is injected to partially expanded vapor inside a volumetric screw expander. This operational strategy has been introduced with the basic functionality and then analysed in depth with an experimental investigation and a modelling approach. Based on that analysis, the following conclusions can be drawn:

- The direct liquid injection is able to reduce the exhaust vapor temperature by up to 40 K depending on the injected mass-flow rate, thus reducing the risk of thermal damages in case of a hermetic or semi-hermetic expander-generator assembly.
- The position where the liquid fluid is injected in the expansion process significantly influences the net power output of the system.
- The net power output of the ORC drops for increased injected mass-flow rates while keeping the operational conditions of the system constant
- For hermetic and semi-hermetic expanders, the reduced exhausted vapor temperatures enables the operation with higher live vapour states by simultaneously ensuring sufficient cooling of the generator.
- The increased live vapour state, can lead to an increase in power production by up to 40 % depending on the operational conditions.
- The next step to finally evaluate the DLI is to test the system with higher live vapor parameter.

Nomenclature

Letter symbols

A	area, m^2
c_p	specific heat, J/(kg K)
C	constant of condenser correlation
$\dot{C}$	capacity flow, W/K
h	specific enthalpy, J/kg
$\dot{m}$	mass flow rate, kg/s
n	number of revolutions, rpm
p	absolute pressure, bar
P	power, W
$\dot{Q}$	heat flow, W
T	temperature, °C
U	heat transfer coefficient, W/(m^2 K)
v	specific volume, m^3/kg
$\dot{V}$	volume flow, m^3/s

Greek symbols

Δ	difference
ε	effectiveness of heat exchanger
η	efficiency
φ	volume ratio

Subscripts and superscripts

c	cold
cond	condenser
D	design conditions
exp	expander
gen	generator
h	hot
int	internal
lv	live vapor
mech	mechanical
p	pump
s	isentropic

References

[1] International Energy Agency. Key World Energy Statistics 2016.

[2] United Nations Framework Convention on Climate Change. Paris Agreement, Conference of the Parties - 21st Session (COP21); December 2015.

[3] Quoilin S, Broek M van den, Declaye S, Dewallef P, Lemort V. Techno-Economic Survey of Organic Rankine Cycle (ORC) Systems. Renewable and Sustainable Energy Reviews 2013; 22:168-86.

[4] Imran M, Usman M, Park B-S, Lee D-H. Volumetric Expanders for Low Grade Heat and Waste Heat Recovery Applications. Renewable and Sustainable Energy Reviews 2016; 57:1090-109.

[5] Bao J, Zhao L. A Review of Working Fluid and Expander Selections for Organic Rankine Cycle. Renewable and Sustainable Energy Reviews 2013; 24:325-42.

[6] Lemort V, Legros A. Positive displacement expanders for Organic Rankine Cycle systems. In: Macchi E, Astolfi M, editors. Organic Rankine Cycle (ORC) Power Systems. Woodhead Publishing; 2017, p. 361-396.

[7] Aumann R, Langer R, Kricke F, Schuster A. Control of ORC Processes by injecting unevaporated fluid (WO 2017 / 00 89 72 A1); 2016.

[8] Declaye S, Quoilin S, Lemort V. Numerical Optimization of an Injection Volumetric Expander for Use in Waste Heat Recovery Organic Rankine Cycle. In: 7th International Conference on Compressors and their Systems, United Kingdom, London, 5-6 September; 2011, p. 375–383

[9] Lemmon, Eric W.; Huber, Marcia L.; McLinden, Mark O.: REFPROP Reference Fluid Thermodynamic and Transport Properties. NIST Standard Reference Database 23, Version 9.1; 2013.

[10] Incropera, Frank P.; DeWitt, David P.; Bergman, Theodore L.; Lavine, Adrienne S.: Fundamentals of heat and mass transfer. 6. ed. Hoboken, NJ: Wiley; 2007.

[11] Lemort, Vincent; Quoilin, Sylvain; Cuevas, Cristian; Lebrun, Jean: Testing and Modeling a Scroll Expander Integrated into an Organic Rankine Cycle. In: Applied Thermal Engineering n. 14-15, 29, pp. 3094–3102. 2009. DOI: 10.1016/j.applthermaleng.2009.04.013.